Supporting Information

Lead-free $BiFeO_3$-$BaTiO_3$ Ceramics with High Curie Temperature: Fine Compositional Tuning across Phase Boundary for High Piezoelectric Charge and Strain Coefficients

Bowei Xun[a], Aizhen Song[a], Jingru Yu[a], Yang Yin[a], Jing-Feng Li[b], Bo-Ping Zhang[a]*

[a]The Beijing Municipal Key Laboratory of New Energy Materials and Technologies, School of Materials Science and Engineering, University of Science and Technology Beijing, 100083 Beijing, China

[b]State Key Laboratory of New Ceramics and Fine Processing, School of Materials Science and Engineering, Tsinghua University, Beijing 100084, China.

* Corresponding author: Bo-Ping Zhang, ORCID: orcid.org/0000-0003-1712-6868; E-mail address: bpzhang@ustb.edu.cn

Supporting Information

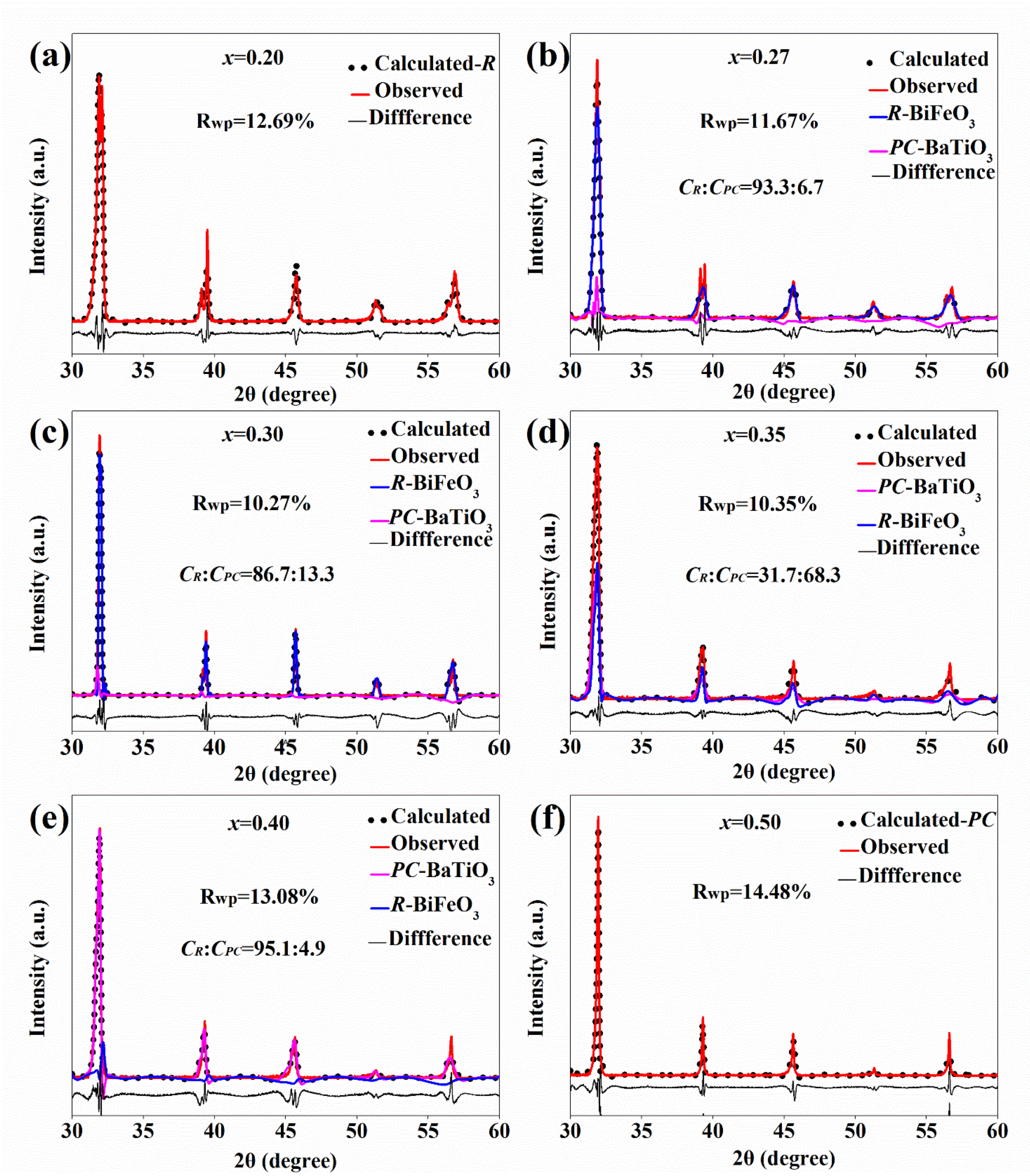

Figure S1 The Rietveld refinement of XRD patterns for (a) BF-0.20BT, (b) BF-0.27BT, (c) BF-0.30BT, (d) BF-0.35BT, (e) BF-0.40BT ceramics and (f) BF-0.50BT ceramics.

Table S1 Rietveld refined lattice parameters and phase ratio of the BF-*x*BT ceramics.

Composition	Phase structure	Space group	Lattice parameters a	b	c	α=β=γ(°)	Reliability fator R_{wp}%	C_R/C_{PC} (%)
BT	*PC*-PDF#75-0461	*Pm*-3*m*	4.012	4.012	4.012	90.00	-	-
BF	*R*-PDF#72-2112	*R*-3*m*	3.952	3.952	3.952	89.60	-	-
0.2	*R*	*R*-3*m*	3.958	3.958	3.958	89.60	12.69	100/0
0.27	*PC*	*Pm*-3*m*	4.011	4.026	3.978	90.00	11.67	93.3/6.7
	R	*R*-3*m*	3.984	3.984	3.984	89.78		
0.30	*PC*	*Pm*-3*m*	3.984	4.014	3.998	90.00	10.27	86.7/13.3
	R	*R*-3*m*	3.979	3.979	3.979	90.22		
0.35	*PC*	*Pm*-3*m*	3.996	4.010	4.024	90.00	10.35	31.7/68.3
	R	*R*-3*m*	4.008	4.008	4.008	90.00		
0.40	*PC*	*Pm*-3*m*	4.006	4.006	4.015	90.00	13.08	4.9/95.1
	R	*R*-3*m*	3.990	3.990	3.990	90.00		
0.50	*PC*	*Pm*-3*m*	3.997	4.008	3.997	90.00	14.48	0/100

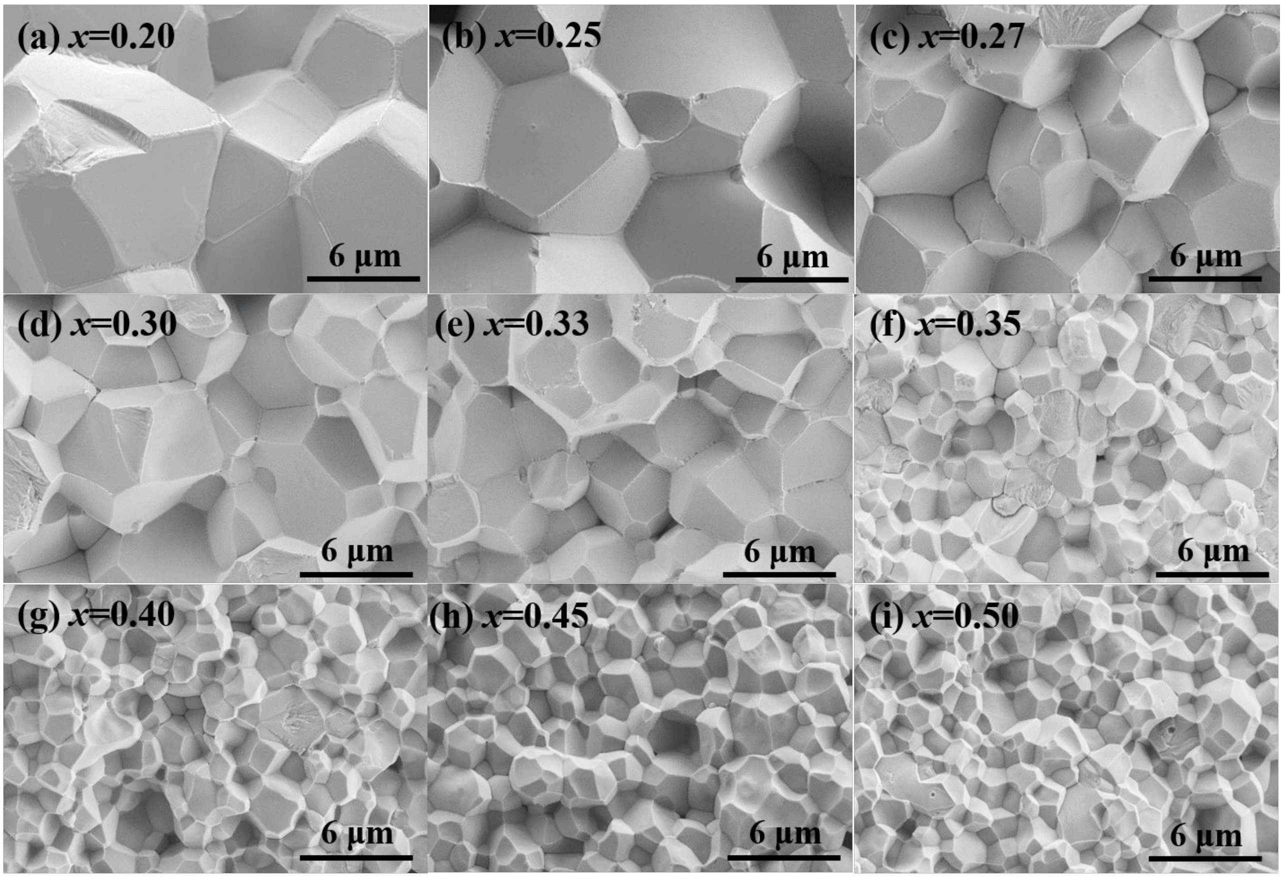

Figure S2 (a-i) SEM images of the fracture surface microstructure of BF-*x*BT ceramics.

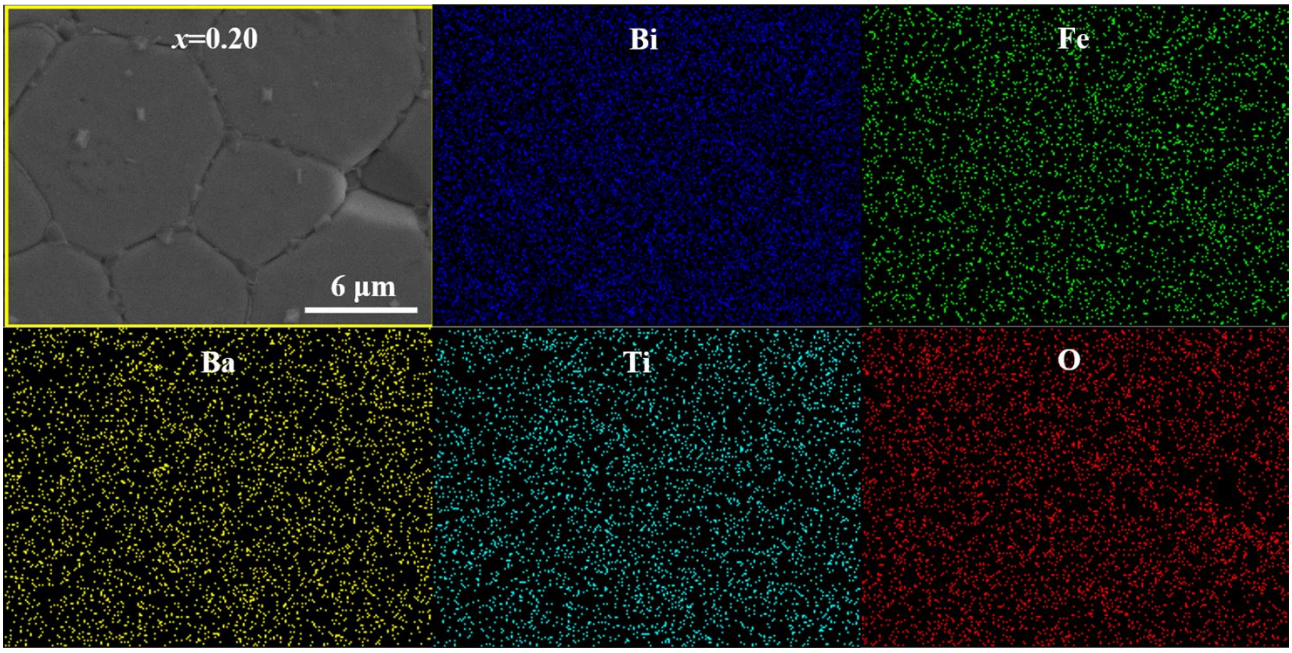

Figure S3 SEM image of the polished surface microstructure of BF-0.20BT ceramic and the energy-dispersive X-ray spectroscopy (EDS) element mapping of BF-0.20BT ceramic.

As shown in Figure S4(a-e), all ceramics exhibit similar electrical behavior within the test temperature range. Firstly, all ceramics show a single arc in the test temperature range, indicating that the grain dominates the ceramic resistance and the effect of grain boundary can be negligible. Secondly, the radius of all semi-arcs (the point of intersection with the Z'-axis) decreases with increasing temperature, indicating the decrease in resistance and the negative temperature coefficient (NTC). Finally, all the ceramics exhibit a flat semicircle with a center below the Z'-axis, indicating the existence of Debye relaxation in ceramics. Generally speaking, the physicochemical properties of grains and grain boundaries are greatly different for polycrystalline ceramics. These two parts generally show different conducting nature. Therefore, two semicircles will be output in AC impedance spectrum, representing the electrical phenomena of grains and grain boundaries respectively.[1-2] The high frequency part on the left is the contribution of grains, and the low frequency part on the right is the contribution of grain boundaries.[3]

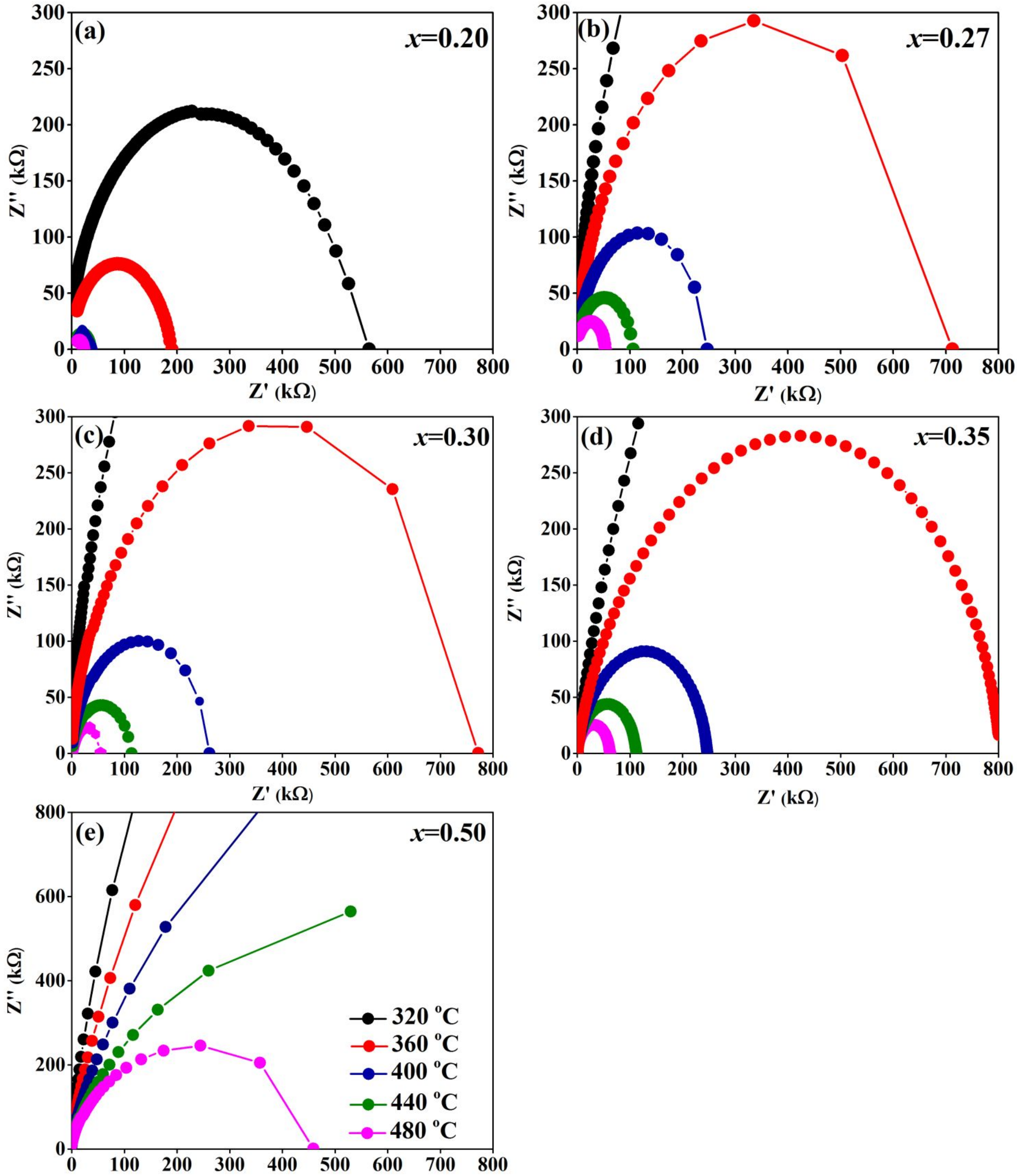

Figure S4 The impedance spectra of (a) x=0.20, (b) x=0.27, (c) x=0.3, (d) x=0.35, (e) x=0.50 ceramics.

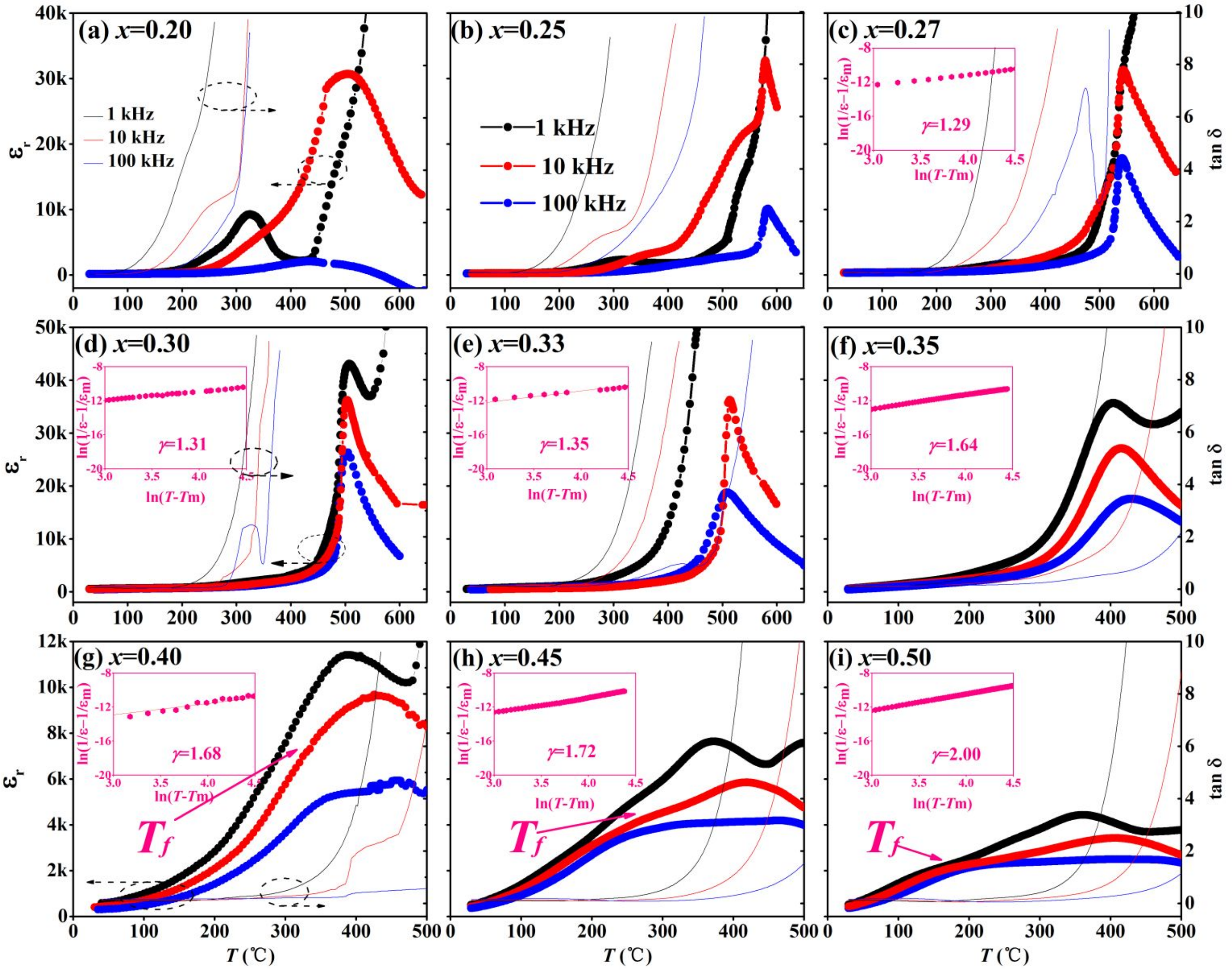

Figure S5 (a-i) The dielectric constant (εr) and loss tangent (tanδ) measured at different frequencies of 1 kHz, 10 kHz, and 100 kHz for BF-xBT ceramics and the dispersion coefficient γ calculated by a modified Curie-Weiss law.

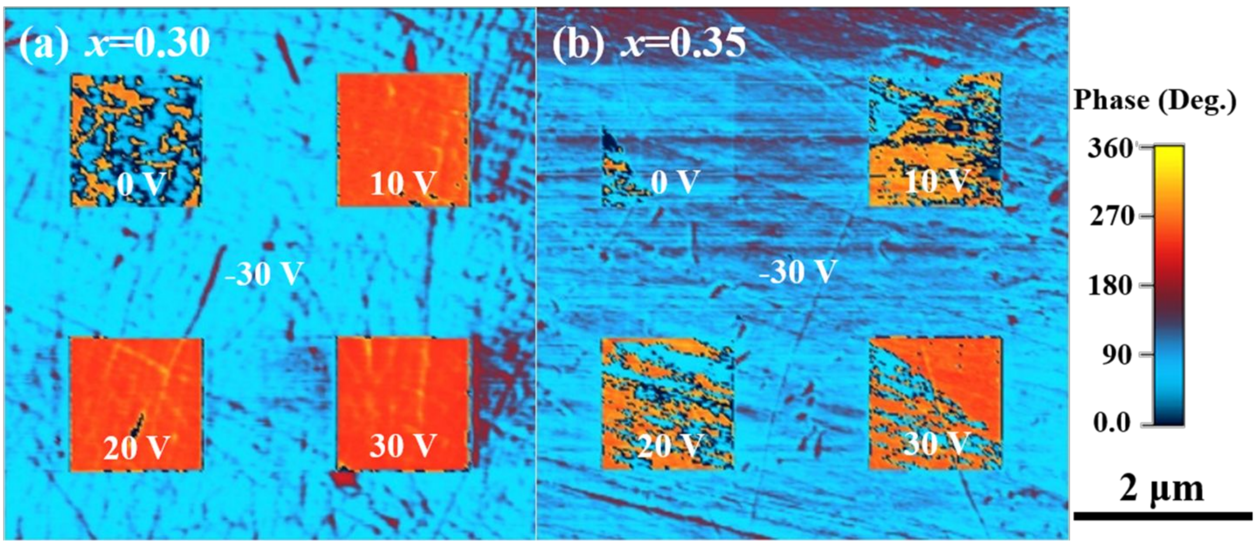

Figure S6 PFM phase images with different electrical voltage for (a) BF-0.30BT and (b) BF-0.35BT ceramics.

(The larger and the smaller squares correspond to 6×6 μm² area and 1.5×1.5 μm² area, respectively).

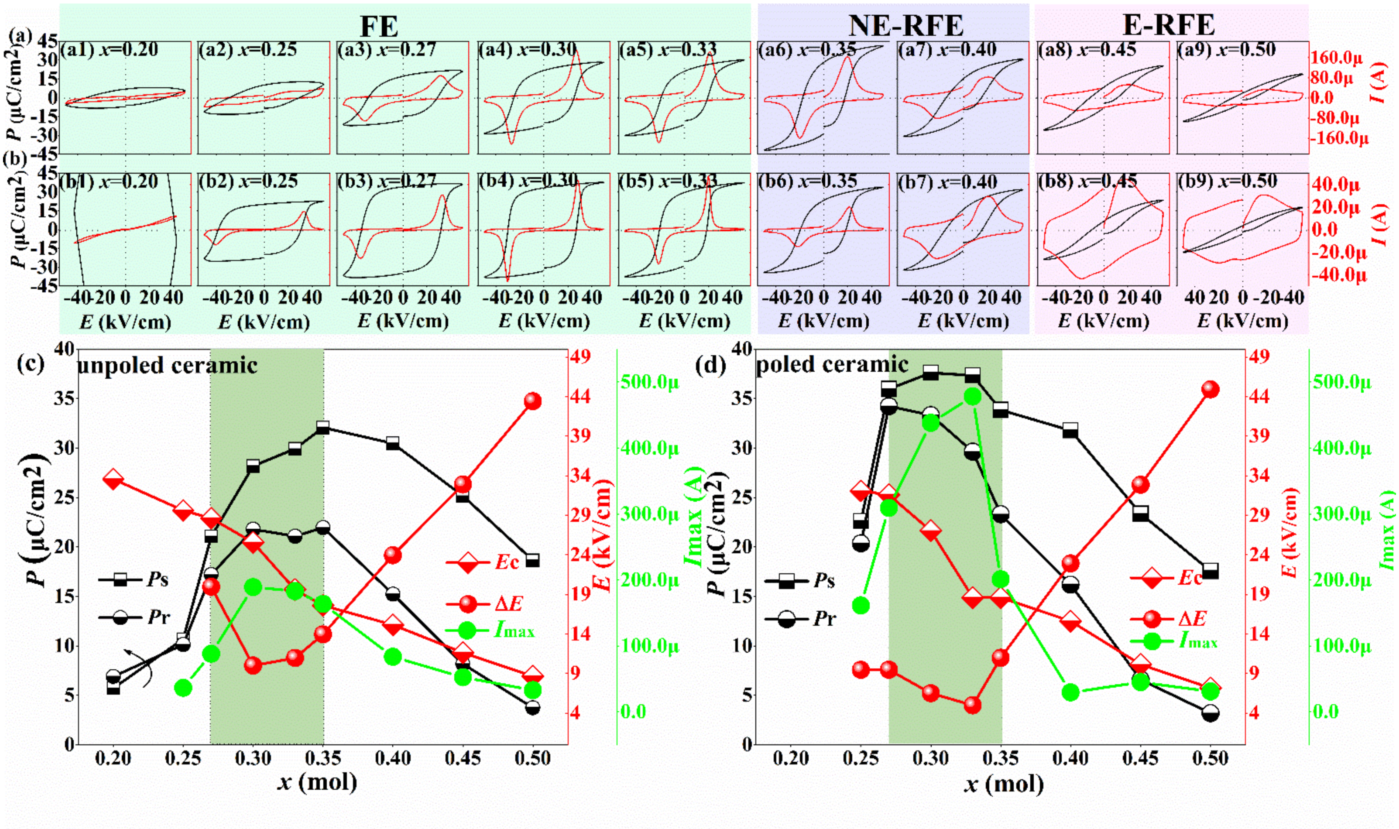

Figure S7 Ferroelectric properties of *P*-*E* and *I*-*E* loops under a 50 kV/cm electric field for (a) unpoled and (b) poled BF-*x*BT ceramics, and P_s, P_r, E_c, I_{max} and ΔE as a function of x for (c) unpoled and (d) poled BF-*x*BT ceramics.

The electrostrictive properties are a good indicator of relaxor characteristics. The S-P^2 curves of the unpoled and poled BF-*x*BT ceramics under a 50 kV/cm electric field are shown in Figure S8(e-f). BF-0.30BT, BF-0.33BT, BF-0.35BT, and BF-0.40BT ceramics do not obey a strictly linear relationship between S and P^2, indicating that electrostrain is mainly attributed to the non-180° ferroelectric domain switching, rather than a simple electrostrictive effect.[4-5] The linearization degree of S-P^2 curves gradually increase with increasing x. The BF-0.45BT and BF-0.50BT ceramics exhibit a linear electrostrictive effect under an applied electric field, which is comparable to classical E-RFE behavior. The relaxor-like electromechanical behaviors are well commensurate with the diffuse dielectric characters, and S-P^2 loops of poled ceramics are consistent with those of unpoled ceramics.

The unipolar *S*-*E* loops of all ceramics exhibit significant hysteresis behavior with varying degrees of hysteresis. Generally speaking, field-induced strain includes not only intrinsic contributions such as field-induced lattice strain and ion movement, but also external contributions, including non-180°domain switching and electric-field-induced transition from relaxation phase to ferroelectric phase.[6] BF-0.25BT, BF-0.27BT, BF-0.30BT, and BF-0.33BT ceramics display obvious negative strains, therefore, the strain hysteresis mainly is caused by irreversible non-180° domain switching. The strain curves of BF-0.35BT and BF-0.40BT ceramics are sigmoidal (Figure S8). The enhanced strain hysteresis appear mainly because the ceramics are in between NE-RFE and E-RFE, and contained both the irreversible non-180° domain switching and the transition from E-RFE to NE-RFE. The strain hysteresis of BF-0.45BT and BF-0.50BT ceramics decrease (Figure S8(g)).

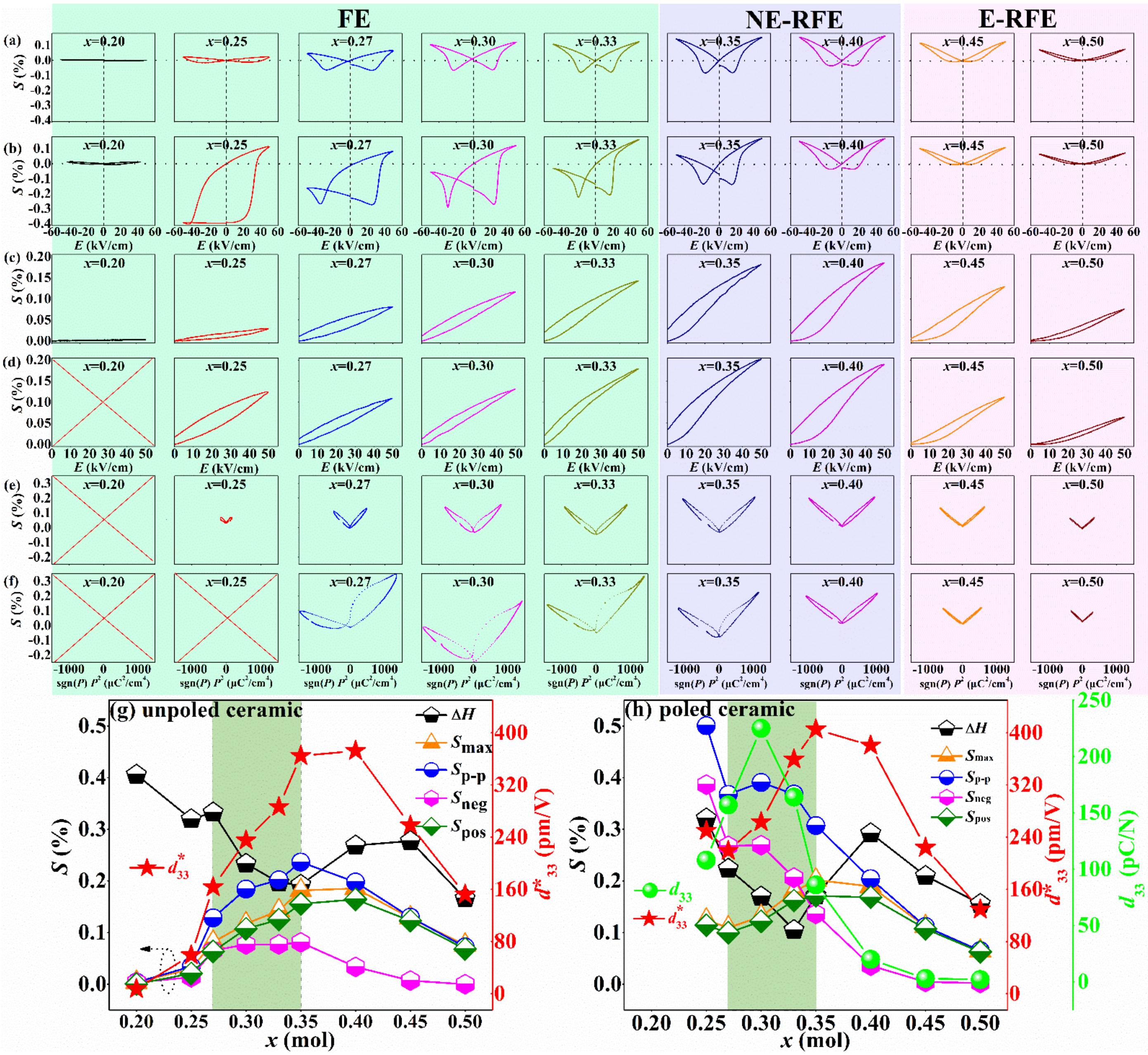

Figure S8 Bipolar strain loops of (a) unpoled and (b) poled BF-xBT ceramics, unipolar strains loops of (c) unpoled and (d) poled BF-xBT ceramics, S-P^2 curves of (e) unpoled and (f) poled BF-xBT ceramics under a 50 kV/cm electric field, and ΔH, S_{max}, $S_{p\text{-}p}$, S_{neg}, S_{pos}, d^*_{33}, and d_{33} as a function of x for (g) unpoled and (h) poled BF-xBT ceramics.

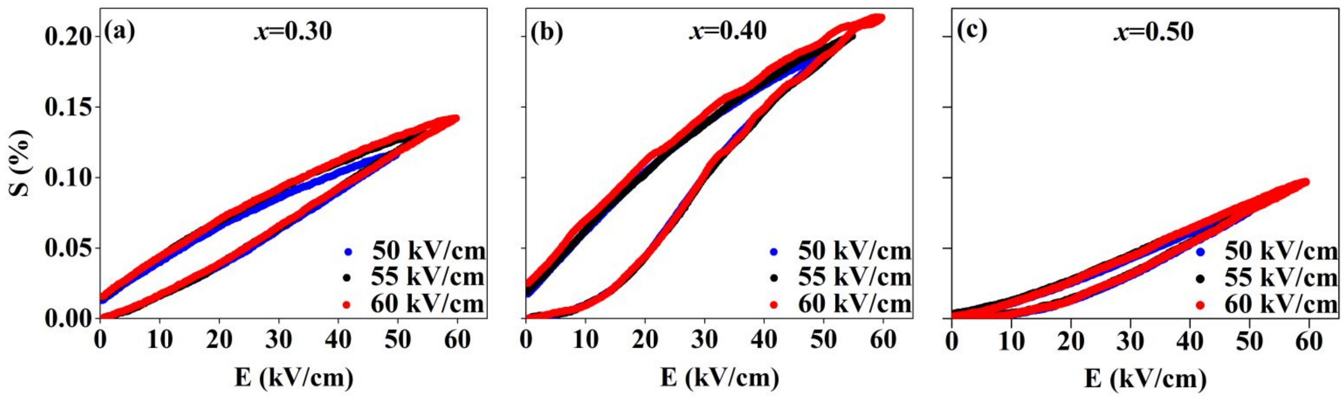

Figure S9 Unipolar strain loops of unpoled (a) BF-0.30BT, (b) BF-0.40BT and (c) BF-0.50BT ceramics under 50 kV/cm, 55 kV/cm and 60 kV/cm.

The unipolar strain loops of unpoled BF-0.30BT, BF-0.40BT and BF-0.50BT ceramics under different electric fields were given in Figure S9. Dielectric breakdown takes place in the piezoelectric ceramics above the electric field of 60 kV/cm. The unipolar strain increased with increasing electrical field, and the loop maintains its shape.

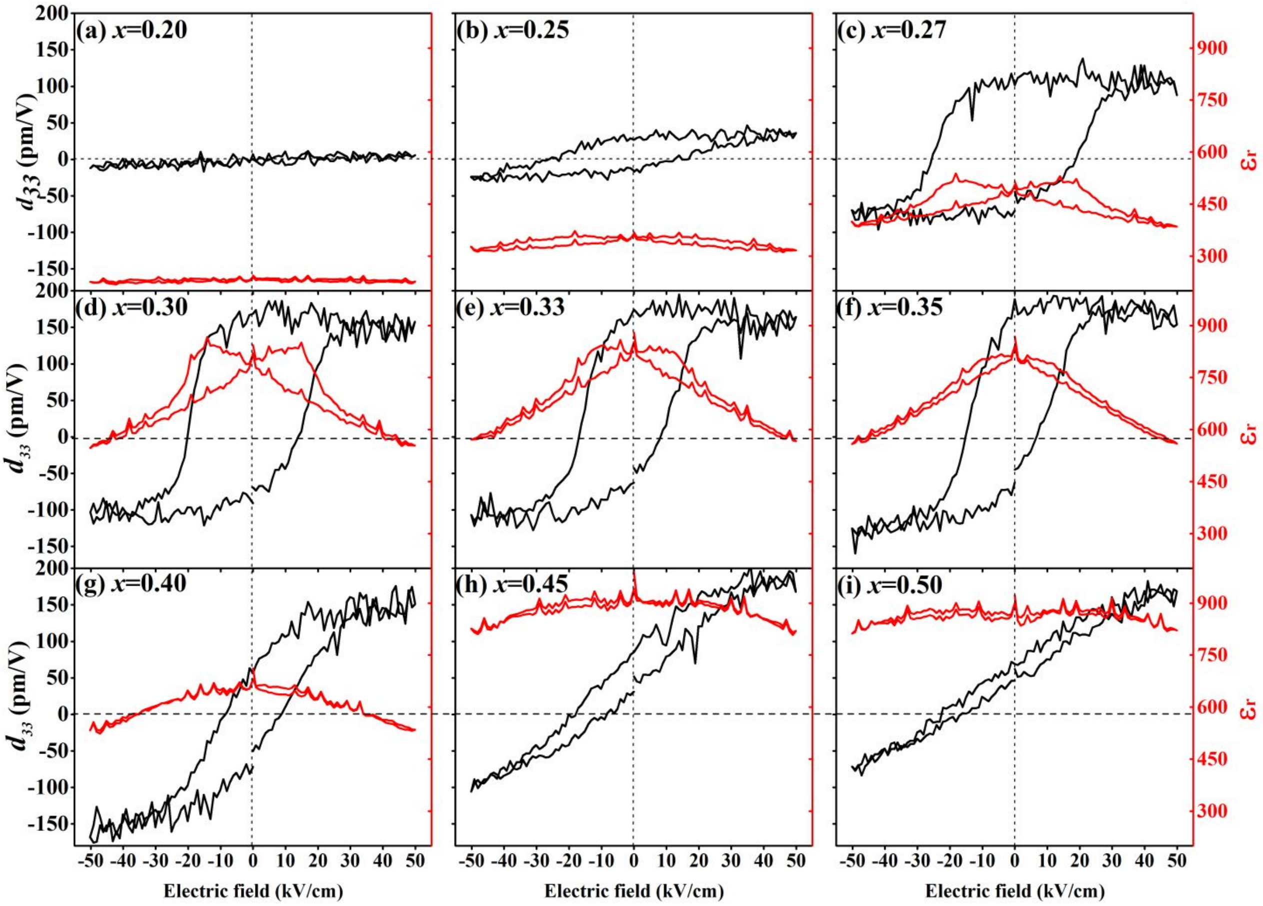

Figure S10 Piezoelectric properties of d_{33}-E and ε_r-E loops under 50 kV/cm electric field for unpoled BF-xBT ceramics ((a) x=0.20; (b) x=0.25; (c) x=0.27; (d) x=0.30; (e) x=0.33; (f) x=0.35; (g) x=0.40; (h) x=0.45 and (i) x=0.50.

Figure S10 shows the d_{33}-E and ε_r-E curves of unpoled BF-xBT ceramics measured under 50 kV/cm. The saturated d_{33}-E loops and the symmetric butterfly-shaped ε_r-E loops are observed in BF-0.27BT, BF-0.30BT, BF-0.33BT and BF-0.35BT ceramics. The ε_r value firstly reaches maximum values near E_C and then drastically decreases with increasing electric field, which corresponds to the process of domain switching.[7-8] However, the d_{33}-E loops of BF-0.40BT, BF-0.45BT and BF-0.50BT ceramics becomes more and more slender, and the butterfly-like ε_r-E curve disappears, the dielectric constant changes little within a wide range of electric field, mainly due to the formation of PNRs.

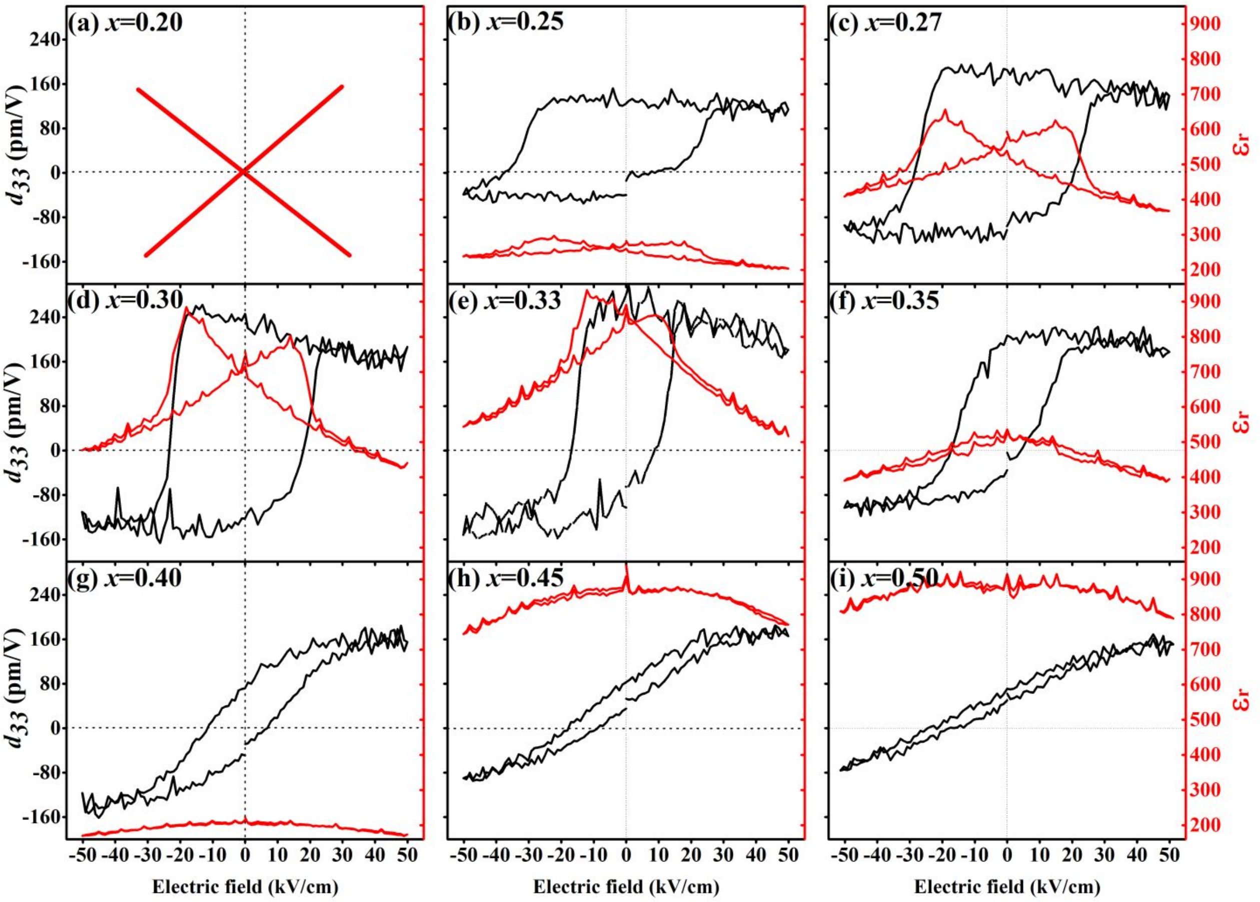

Figure S11 Piezoelectric properties of d_{33}-E and ε_r-E loops under 50 kV/cm electric field for poled BF-xBT ceramics ((a) x=0.20; (b) x=0.25; (c) x=0.27; (d) x=0.30; (e) x=0.33; (f) x=0.35; (g) x=0.40; (h) x=0.45; (i) x=0.50).

Figure S11 presents the d_{33}-E and ε_r-E curves of poled BF-xBT samples measured under 50 kV/cm. The d_{33}-E loops of poled BF-0.25BT, BF-0.27BT, BF-0.30BT and BF-0.33BT samples are more saturated than those of unpoled ceramics. Meanwhile, the asymmetric butterfly-shaped ε_r-E loops are also observed. By the discussion above, the domains of poled ceramics are easier to switch under the measure electric field than unpoled ceramics. In addition, most of the domains and defect dipoles are arranged along the direction of electric field, leading to the establishment of an internal bias electric field (E_i) in the grains. Therefore, ferroelectric domain dynamics is a pretty vital factor to affect the piezoelectric properties of ceramics. The d_{33}-E and ε_r-E curves of poled BF-0.40BT, BF-0.45BT and BF-0.50BT ceramics show little change due to the formation of reversible PNRs.

Conflicts of interest

There are no conflicts of interest to declare.

Acknowledgements

This work was supported by National Natural Science Foundation of China (grant no.52032007 and 52072028)

References

(1) Kumar, M.; Shankar, S.; Kumar, S.; Thakur, O.; Ghosh, A. K. Impedance spectroscopy and conductivity analysis of multiferroic BFO–BT solid solutions. *Physics Letters A* **2017,** *381* (4), 379-386.

(2) Singh, H.; Kumar, A.; Yadav, K. Structural, dielectric, magnetic, magnetodielectric and impedance spectroscopic studies of multiferroic $BiFeO_3$–$BaTiO_3$ ceramics. *Materials Science and Engineering: B* **2011,** *176* (7), 540-547.

(3) Deng, X.-Z.; Zhang, L.-Y.; Geng, X.-Y.; Zhang, J.; Sun, L.; Wang, R.-X.; Gu, Z.-B.; Zhang, S.-T. Crystal structure, impedance, and multiferroic property of $SrZrO_3$ and MnO_2 modified $0.725BiFeO_3$−$0.275BaTiO_3$ ceramics. *Ceramics International* **2017,** *43* (17), 14748-14755.

(4) Liu, X.; Zhai, J.; Shen, B. Novel bismuth ferrite-based lead-free incipient piezoceramics with high electromechanical response. *Journal of Materials Chemistry C* **2019,** *7* (17), 5122-5130.

(5) Kuwata, J.; Uchino, K.; Nomura, S. Electrostrictive coefficients of Pb $(Mg_{1/3}Nb_{2/3})O_3$ ceramics. *Japanese Journal of Applied Physics* **1980,** *19* (11), 2099-2103.

(6) Wang, L.; Liang, R.; Zhou, Z.; Dong, X. High electrostrain with high Curie temperature in $BiFeO_3$-$BaTiO_3$-based ceramics. *Scripta Materialia* **2019,** *164*, 62-65.

(7) Zhang, M.; Zhang, X.; Qi, X.; Zhu, H.; Li, Y.; Gu, Y. Enhanced ferroelectric, magnetic and magnetoelectric properties of multiferroic $BiFeO_3$–$BaTiO_3$–$LaFeO_3$ ceramics. *Ceramics International* **2018,** *44* (17), 21269-21276.

(8) Yao, F. Z.; Wang, K.; Jo, W.; Webber, K. G.; Comyn, T. P.; Ding, J. X.; Xu, B.; Cheng, L. Q.; Zheng, M. P.; Hou, Y. D. Diffused phase transition boosts thermal stability of high−performance lead−free piezoelectrics. *Advanced Functional Materials* **2016,** *26* (8), 1217-1224.